Atmósfera (2002) 15, pp. 1-18

An explosive cyclogenesis over land

NORMA E. POSSIA

Departamento de Ciencias de la Atmósfera, Centro de Investigaciones del Mar y la Atmósfera (CIMA), CONICET/UBA, Buenos Aires, Argentina

(Manuscript received, July 3, 2000; accepted in final form April 3, 2001)

RESUMEN

Este trabajo realiza un estudio analítico de una ciclogénesis explosiva ocurrida entre el 11 y 12 de noviembre de 1989, en el noreste de la Argentina. A través de los datos provenientes de los análisis del ECMWF, se evalúan los términos de las ecuaciones que gobiernan el movimiento atmosférico, para establecer los mecanismos detonantes de la misma.

Esta ciclogénesis comienza con procesos de altura clásicos, tales como la advección de vorticidad y divergencia. A los mismos, se asocian rápidamente los procesos diabáticos, creando fuerte vorticidad potencial ciclónica en niveles bajos y destruyendo la misma en niveles altos. El gran desarrollo se produce cuando la vorticidad ciclónica en altura permanece a pesar de los mecanismos que la debilitan.

ABSTRACT

In this paper, an analytical study of an explosive cyclogenesis that occurred in northeastern Argentina on 11-12 November 1989, is carried out. European Centre for Medium Range Weather Forecasts Analysis data are used to compute the terms of the atmospheric motion governing equations in order to determine the triggering mechanisms of this event.

This cyclogenesis is initiated by classical processes such as the advection of vorticity and divergence in the upper troposphere. The diabatic mechanisms rapidly associate to these processes, generating an intense cyclonic potential vorticity in low levels and depleting it in upper levels. The major development occurs when the presence of cyclonic vorticity in upper levels continues in spite of the mechanisms tending to weaken it.

Key words: explosive cyclogenesis, rapid cyclogenesis, Bomb.

1. Introduction

Among the numerous investigations concerning explosive cyclogenesis, that of Sanders and Gyakum (1980) occupies a relevant position because these authors give a definition of such systems as well as outlines their predominant characteristics. They define these systems of rapid development as "Bomb" when the decrease of the pressure in 24 hours multiplied by the ratio between the sine of 60°and the sine of the latitude at the event is greater or equal to one. The above mentioned study, performed for the Northern Hemisphere and the period September 1976 to May 1979, indicates that in most of the cases the cyclogenesis are maritime, occur during the cold season and have as main energy source the Sea Surface Temperature and its strong gradients. Moreover, they are associated to a large divergence in upper levels.

The cases of explosive cyclogenesis that occur over land are less frequent. Ruscher and Condo (1996) note the existence of few studies on the subject, and associate this fact not only to their rareness but also to the lack of agreement about their generation mechanisms.

In this paper, an intense cyclogenesis occurred on continental area has been chosen for a case study. It occurred on November 11-12, 1989 in northeastern Argentina and was characterized by an extraordinarily rapid development. Because of its intensity, rapid development, and the generated related economic loss, this case has deserved previous studies. Gordillo *et al.* (1991) study the prevision of the southeastern wind storm over the River Plate by means of simple diagnostic techniques. Seluchi and Saulo (1998) use a regional model to analyze the physical mechanisms responsible for this development; they conclude that the diabatic processes played an important role in the rapid deepening of the system.

The aim of this paper is to study the mechanisms relevant to this development. European Centre for Medium Range Weather Forecasts (ECMWF) analysis data are used to evaluate the governing equations and determine the relative importance of each term.

2. The synoptic situation

The cyclogenesis occurred over a frontal zone located northeast the Río de la Plata. It started between 12 and 18 UTC, 11 November and reached its maximum depth at 18 UTC the next day. It can be considered an explosive cyclogenesis (Seluchi and Saulo, 1998) as the pressure decreased 26 hPa within a period of 24 hours after 12 UTC, 11 November. When the pressure decreases much stronger that this one, it occurs at higher latitudes than 32°S.

2.1 The data set

The data used to perform the calculations are the ECMWF high resolution (every 1.125°), six-hourly analysis data. These data have 7 pressure levels at 1000, 850, 700, 500, 300, 200 and 100 hPa. Additional information, provided by the Argentine National Weather Service is used in order to include the related meteorological observations during the event.

2.2 Description of the meteorological situation

The 1000 hPa geopotential together with the 1000/500 thickness field for November, 11-12, 1989 are shown in Figure 1. At 12 UTC, 10 November there is a thickness wave with a length of 25°, with a cold tongue over the Pacific coast and higher values of thickness over the continent; this is a favorable situation for cyclogenesis at northeastern Argentina (Seluchi, 1995). Cumulonimbi and thunderstorms are reported by the meteorological stations located at central Argentina. The Patagonia is under the effects of an intense advection of cold air and the influence of a through that culminates with a closed center north of Malvinas Islands.

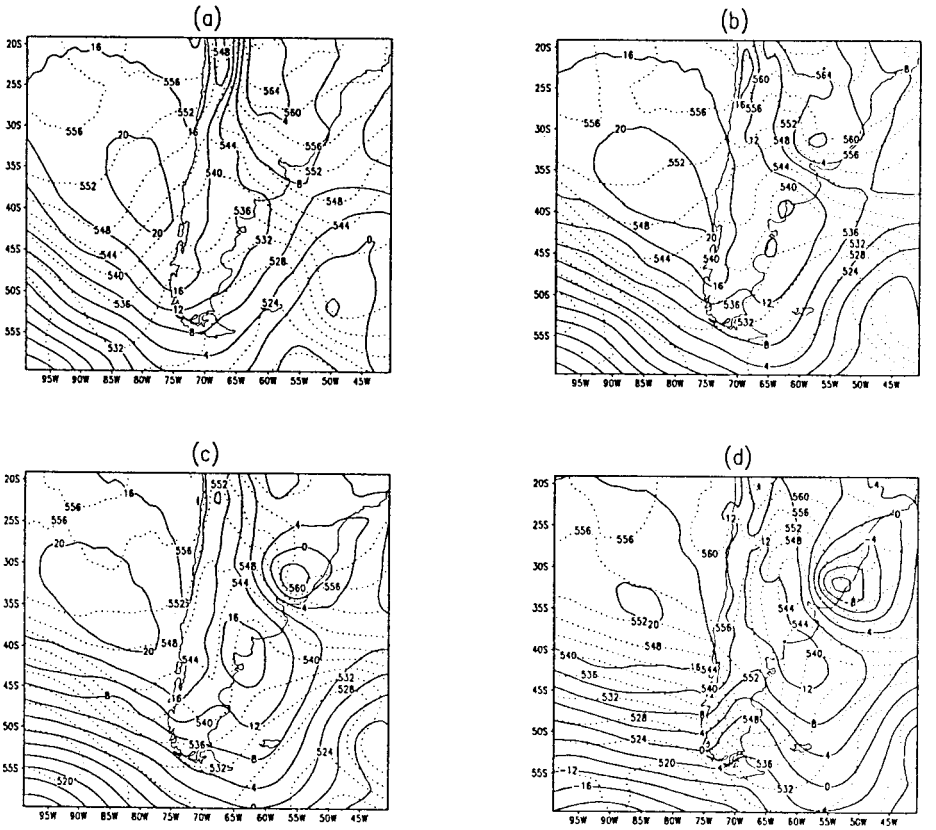

Fig. 1. ECMWF analyses of 1000 hPa geopotential height (—) and 1000/500 and thickness (. . . .) at: a) 12 UTC 11 November 1989, b) 00 UTC 12 November 1989, c) 06 UTC 12 November 1989 and d) 18 UTC 12 November, 1989.

After 24 hours (Fig. 1a) a high pressure system begins to penetrate into the continent in the south. The Río de la Plata region is dominated by high values of thickness, meanwhile they decreased over western Argentina. At 00 UTC, 11 November (Fig. 1b), there is a closed low pressure center over Uruguay related to intense winds of around 35 kt. Even when the cyclonic system begins within a baroclinic field, its intensification to the south-west of the center as well as the penetration of values of thickness typical of tropical air towards the center are remarkable. It can be seen in Figure 1c, that the anticyclone formed over the Patagonia during the previous hours reaches the Atlantic coast and the low pressure center increased its intensity.

By this time (06 UTC), the three-hourly tendency in the low-pressure center attains the value of -4.9 hPa and the winds at the Uruguayan coast reach 40 kt. Afterwards, the low-pressure system elongates toward the east and continues its intensification meanwhile the anticyclone advances over the Atlantic coast and the winds increase over the Río de la Plata (Fig. 1d).

Intense precipitation occurred over eastern Argentina and Uruguay; the values registered within the area of maximum intensification of the system between November 11 and 12 at 12 UTC exceeded 100 mm, indicating a caloric energy release of 2.5 $\times 10^8$ J m^{-2}.

The equivalent potential temperature (θ_e) fields are computed in order to analyze the synoptic situation at low level; they are calculated with the equation suggested by Bolton (1980). Results at 850 hPa are shown in Figure 2. Two areas of strong gradients of θ_e are present at 00 UTC 10 November, one is located over the southern Patagonia and the other one, more intense, over the north central region of Argentina and Uruguay with high potential temperatures penetrating southward over northwestern Argentina. At 06 UTC 12 November, (Fig. 2), air with an equivalent potential temperature of 345 K moves from Paraguay to Uruguay, reaching the center of the cyclone. Besides, the entrance of potentially colder air from the south is clearly visible over the Río de la Plata, giving place a zone of strong gradients of θ_e.

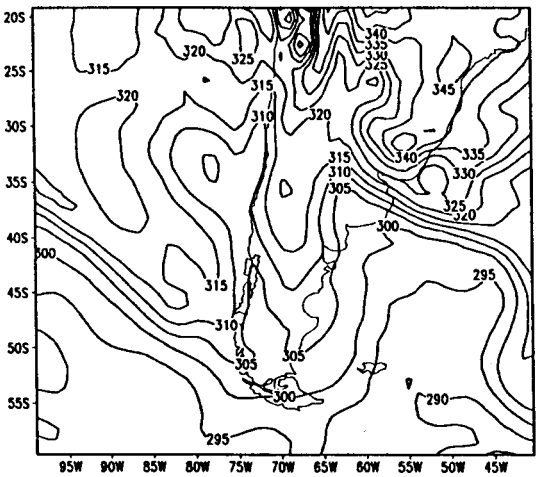

Fig. 2. Equivalent potential temperature (θ_e) at 850 hPa at 06 UTC 12 November.

The geopotential and temperature fields at 500 hPa for 0 UTC 10 November, are shown in Figure 3, in which a trough located at 80°W and between 35 and 60°S can be observed. At 0 UTC November 11 (Fig. 3b), the southern portion of the trough is located between 60 and 55°W, meanwhile the northern part has not entered to the continent yet. Twelve hours later (Fig. 3c), the whole system is over the continent

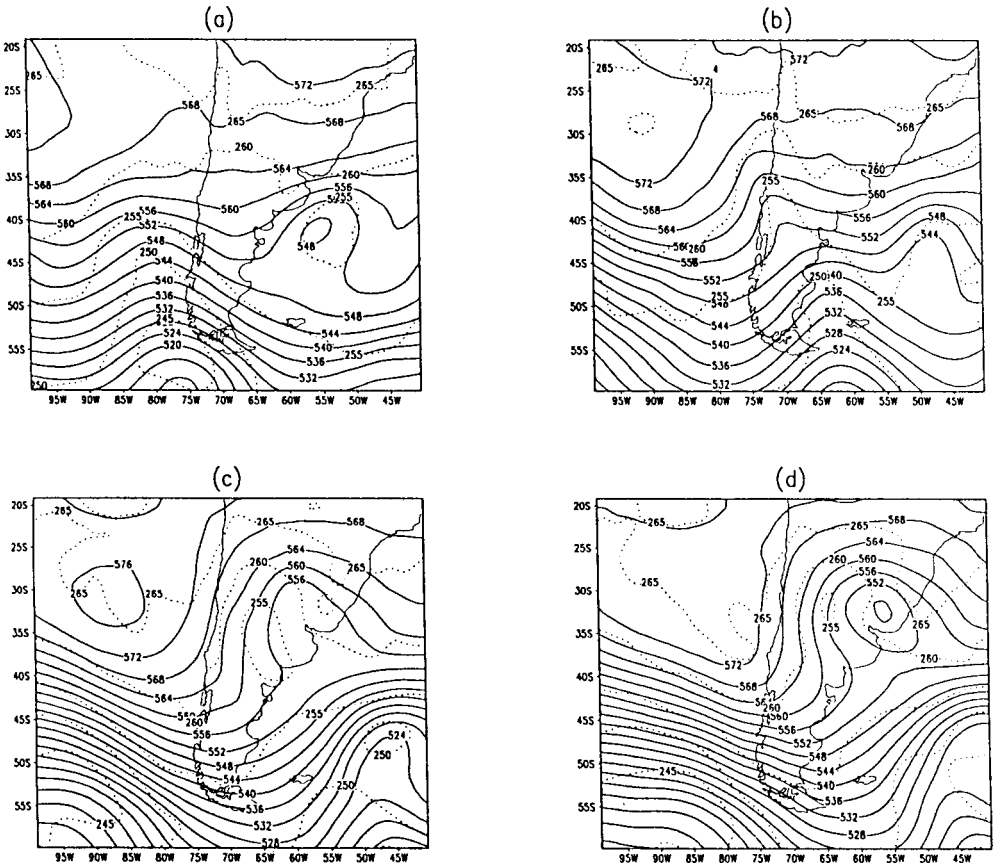

Fig. 3. ECMWF analyses of 500 hPa geopotential height (—) and temperature (. . . .) at: a) 00 UTC 10 November, b) 00 UTC 11 November, c) 06 UTC 12 November and d) 12 UTC 12 November.

and the temperature wave lags the one of the geopotential. The deepening of the trough is very significant during these 12 hours. There is a closed center over Uruguay extending form the surface up to 300 hPa at 12 UTC (Fig. 3d), that continues its deepening until 18 UTC. After that time, the system begins its weakening as it moves eastward with a slight northward component.

At 300 hPa, the system exhibits a behavior similar to that corresponding to 500 hPa. In Figure 4a the relative vorticity field for 06 UTC, 11 November is shown. A process of elongation towards the east begins on 12 November, 12 UTC; it is related to the low pressure closed center mentioned previously (Fig. 4b). The divergence fields at 300 hPa show an increase of 8×10^{-5} s^{-1} from 00 to 06 UTC when it reaches its maximum value of 11×10^{-5} s^{-1} (Fig. 5). It is interesting to analyze the divergence and the vertical velocity evolution together (Fig. 6). This last variable also increases along those 6 hours from 1 Pa s^{-1} to a maximum value of 3 Pa s^{-1}.

The wind speed at 300 hPa for 12 UTC, 11 November is shown in Figure 7; here the penetration of a jet stream from the Pacific Ocean to the west of the cyclogenesis and another one going out towards the Atlantic can be seen.

The vertical section at 32.5°S of the potential temperature for 06 UTC 12 November (Fig. 8), shows that the system under study is located at 56°W and has a warm center and therefore the lowering of the tropopause is less than 50 hPa.

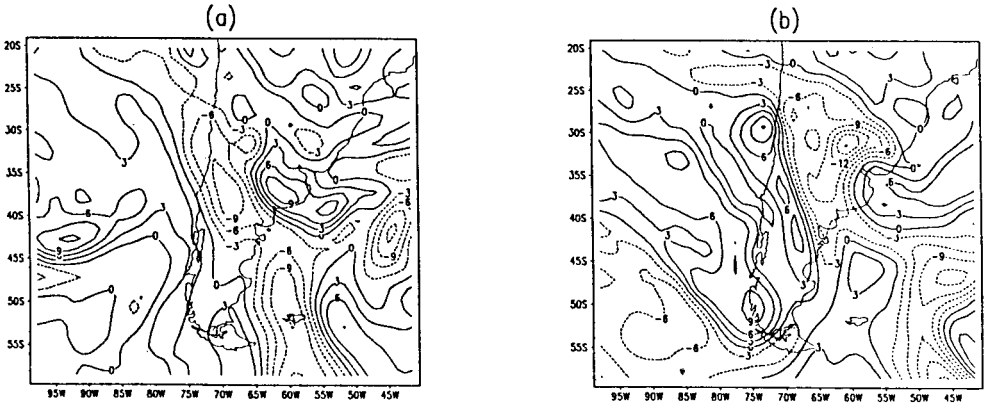

Fig. 4. Relative vorticity field at 300 hPa at: a) 06 UTC 11 November and b) 06 November. Contours are labelled in 3×10^{-5} s^{-1}.

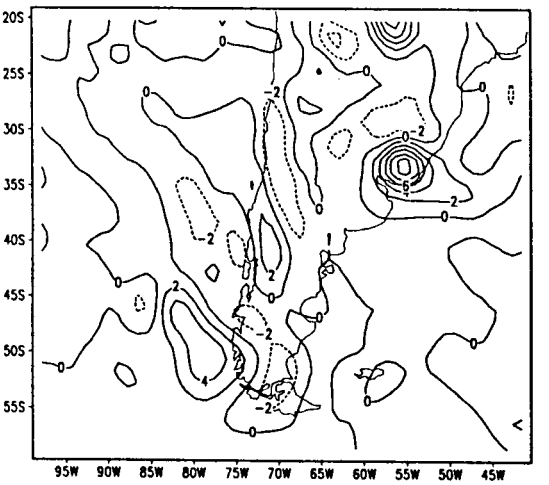

Fig. 5. Divergence field at 300 hPa at 06 UTC 12 November. Contours are labelled in 3×10^{-5} s^{-1}.

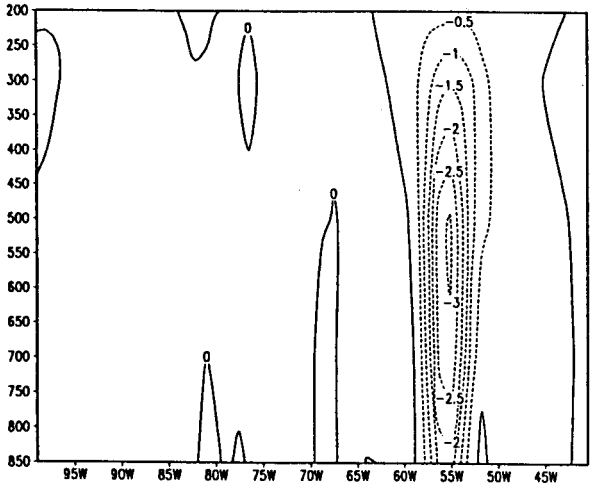

Fig. 6. Zonal vertical cross section at 32.5°S of the vertical velocity (Pa s^{-1}) at 06 UTC 12 November.

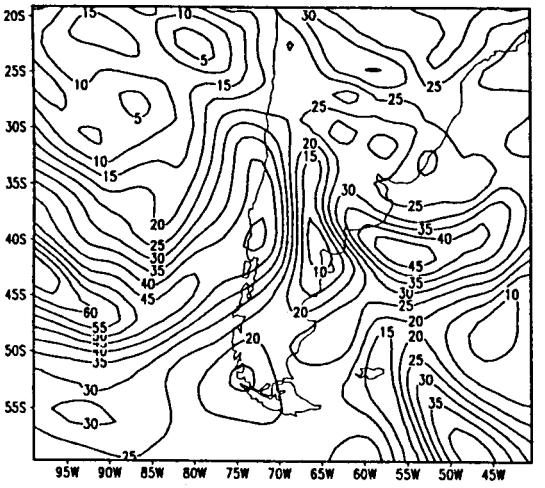

Fig. 7. Wind speed (m s^{-1}) at 300 hPa at 12 UTC 11 November.

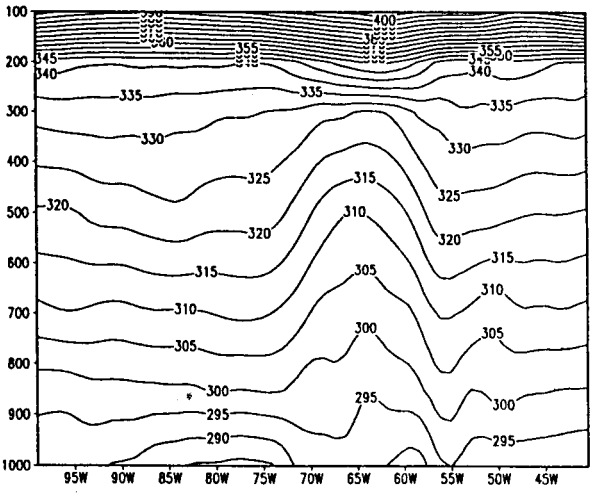

Fig. 8. Zonal vertical cross section at 32.5°S of the potential temperature at 06 UTC 12 November.

3. Analysis of the cyclogenesis factors

In order to determine which process prevails during every of the cyclogenesis stages, the terms of the vorticity and thermodynamic equations were computed. As a synthesis of them, the evolution of the potential vorticity was also evaluated, following the methodology proposed by Lau and Lau (1992), except that in this case it is applied to a particular situation.

Second order centered differences were used to compute the spatial derivatives. For the temporal derivatives, as data were available six hourly, and the CFL criterion indicates that the time step should be lower than half an hour, the values were interpolated using a backward Gauss polynomial of fourth order (Gerald, 1978), and then centered fourth order differences were applied.

3.1 Dynamical factors

In order to identify the beginning of the perturbation, Hovmöller diagrams at 1000, 850, 700, 500 and 300 hPa were drawn, the ones corresponding to relative vorticity at 32.5°S being shown in Figure 9. It can be seen that the cyclonic perturbation begins at upper levels during the 10 November at approximately 06 UTC, meanwhile at the other levels, the first negative contour appears 12 hours later. The weakest vorticity fields are located at 500 hPa, significantly increasing its intensity descending to the level of 850 hPa. This is a characteristic of the cyclonic systems with warm center, and in this case the largest increase of thickness is located between 850 and 700 hPa. The weakening of the vorticity below 850 hPa is remarkable. At 850, 700 and 300 hPa, two centers in which the system rapidly develops can be identified within the cyclonic perturbation.

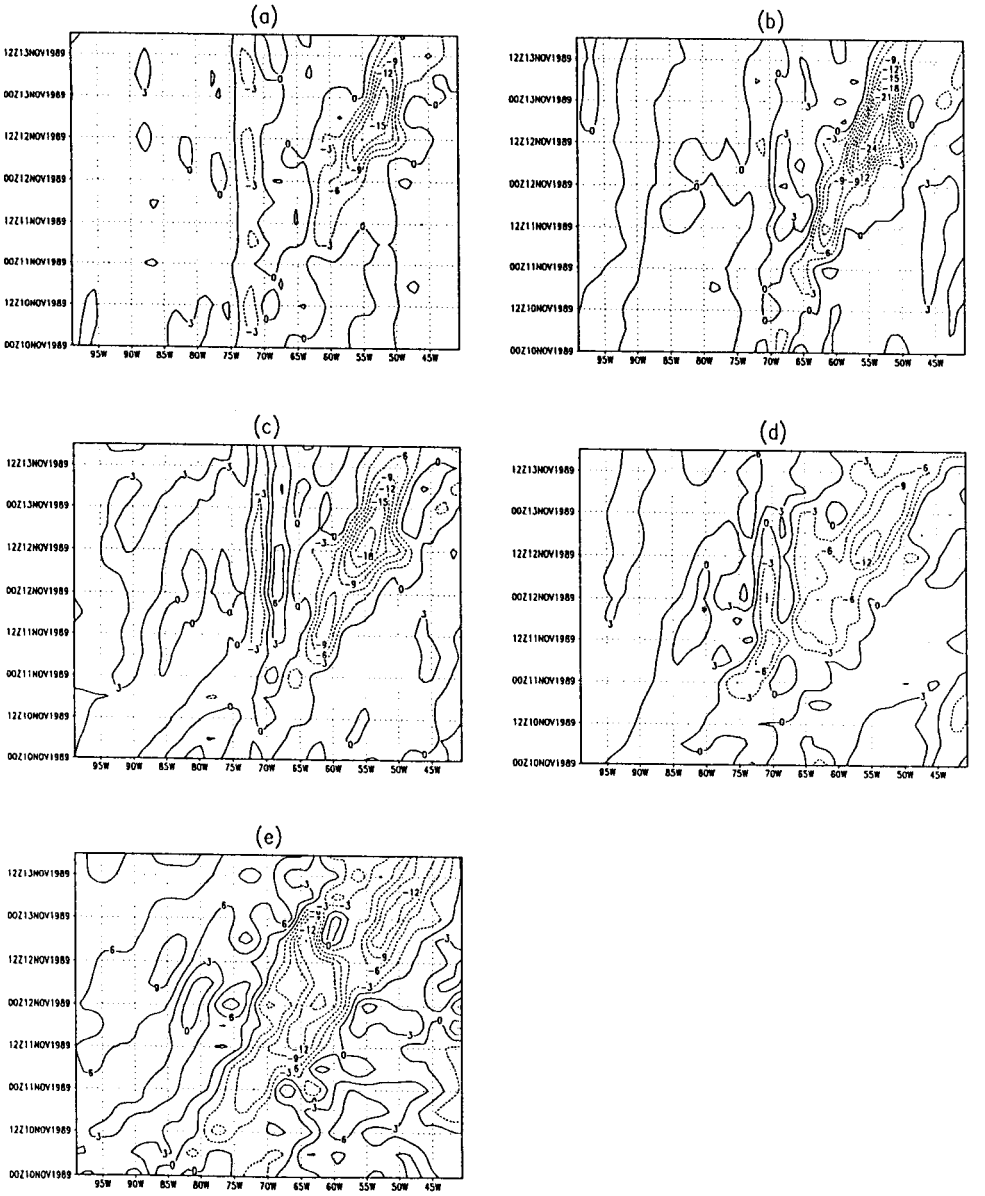

Fig. 9. Hovmöller diagrams for relative vorticity at 32.5°S for a) 1000 hPa, b) 850 hPa, c) 700 hPa, d) 500 hPa and e) 300 hPa. Contours are labelled in 3×10^{-5} s^{-1}.

In order to identify the dynamical processes that originated the situation under study, the temporal evolution equation for the relative vorticity is used:

$$\frac{\partial \zeta}{\partial t} = -\mathbf{V}_H \cdot \nabla_\zeta - \omega \frac{\partial \zeta}{\partial p} - \mathbf{k} \cdot (\nabla \omega \times \frac{\partial \mathbf{V}_H}{\partial p}) - (\zeta + f) \nabla \cdot \mathbf{V}_H - \beta v \tag{1}$$

where: ζ is the vertical component of the relative vorticity,

$\mathbf{V}_H$ the horizontal wind,

∇ the nabla differential operator for constant pressure,

$\mathbf{k}$ the vertical versor,

ω the vertical velocity in the isobaric system,

f the Coriolis parameter,

β the Rossby parameter, and

v the meridional component of the wind.

Every term of the right hand side of equation (1) is evaluated for each of the 7 pressure levels of the ECMWF analysis data. The so obtained results, including for each term the minus sign that precedes them are represented in the following graphs (Figs. 11- 14).

In order to complement Figure 9, Hovmöller diagrams at 32.5°S for $\partial\zeta/\partial t$ are shown in Figure 10; in this last figure values lower than -3×10^{-11} s^{-2} are shaded. This diagram helps on identifying the place and time at which the cyclonic intensification is most rapid, and may be related to physical processes.

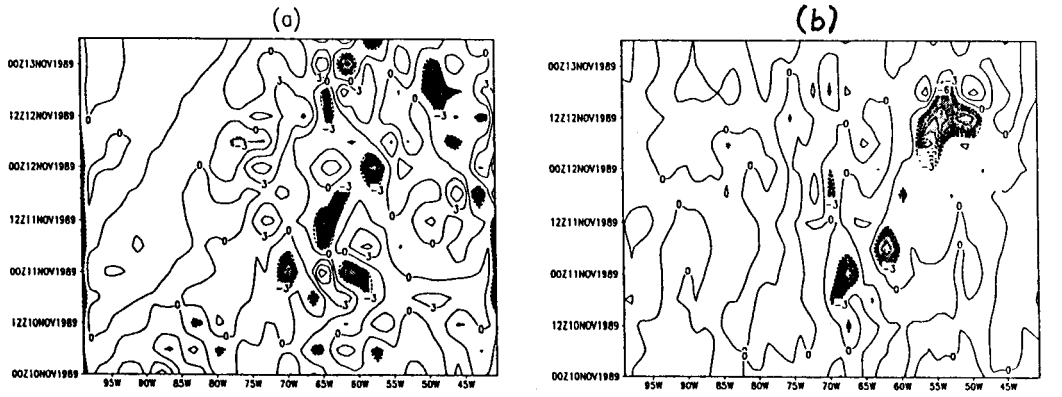

Fig. 10. Hovmöller diagrams for local variations of relative vorticity at 32.5°S for a) 850 hPa and b) 300 hPa. Contours are labelled in 3×10^{-9} s^{-2}.

At 300 hPa as well as at 850 hPa, the first intense case of cyclonic intensification occurs around 00 UTC of 11 November. At 300 hPa, there are three centers of interest related to the cyclonic perturbation of Figure 9; all of them are previous to the time of maximum development of the system. The first one is at 00 UTC 11 November, centered at 70°W, the second at 65°W at 12 UTC of the same day and last one at 58°W at 00 UTC of 12 November. The most important terms related to the formation of these centers are computed as discussed before.

The horizontal advection fields of relative vorticity at 300 hPa are shown in Figure 11. At 12 UTC 11 November, there is an anticyclonic vorticity advection center of 8×10^{-9} s^{-2} over the Pacific coast moving northeastward, meanwhile values of cyclonic vorticity advection of the same intensity are present

at central and eastern Argentina. At 00 UTC 11 November, the anticyclonic vorticity advection persist over the western of the continent, meanwhile the cyclonic advection has increased, extended and moved northeastward (Fig. 11b). This latter center weakens along the following hours.

Some results for the divergence term at 300 hPa are given in Figure 12. At 06 UTC, 11 November the divergence term reaches a value of 5×10^{-9} s^{-2} (Fig. 12a), and then weakens to reinforce at 00 UTC 12 November. This term reaches a maximum of 12×10^{-9} s^{-2} at 06 UTC (Fig. 12c). During the subsequent 12 hours the positive center gradually weakens and is surrounded by negative values.

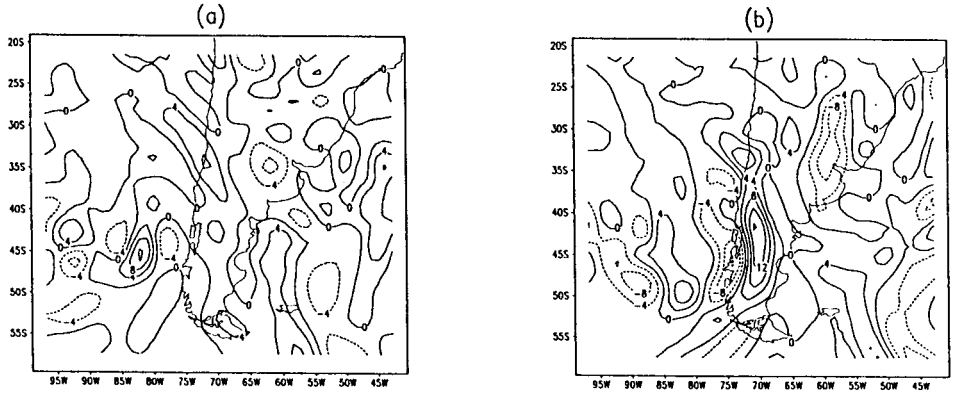

Fig. 11. Horizontal advection of relative vorticity at 300 hPa at: a) 12 UTC 11 November and b) 00 UTC 12 November. Contours are labelled in 4×10^{-9} s^{-2}.

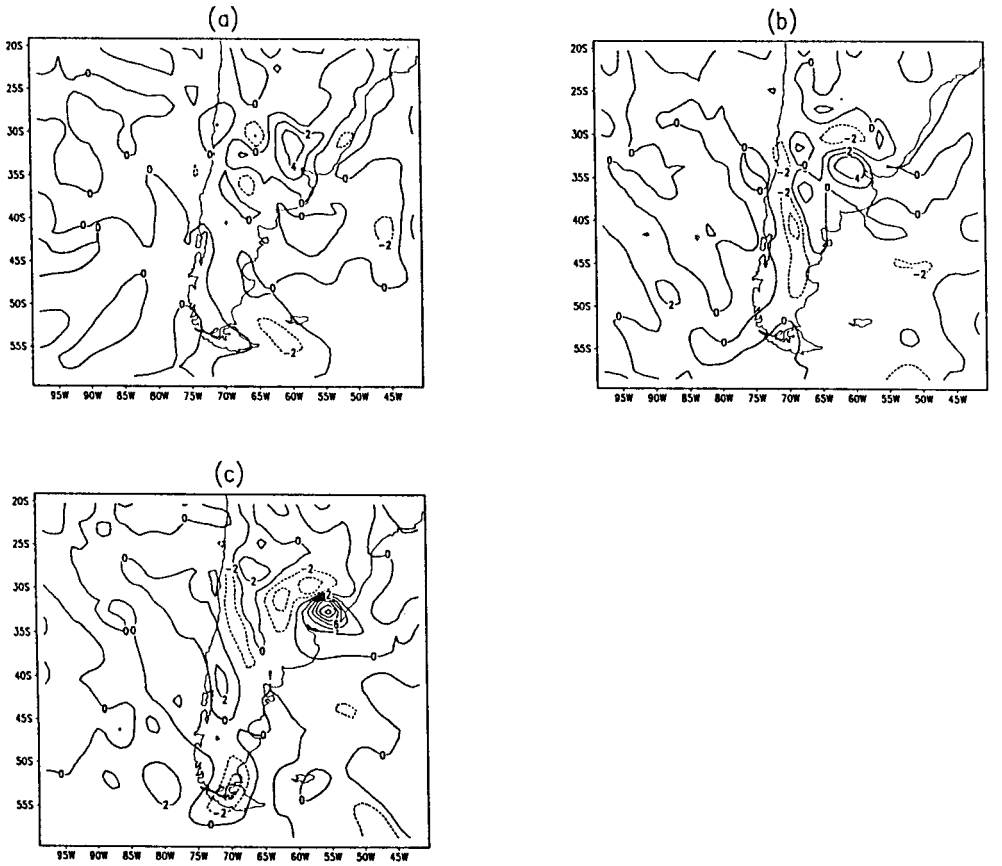

Fig. 12. Divergence term at 300 hPa at: a) 06 UTC 11 November and b) 06 UTC 12 November. Contours are labelled in 2×10^{-9} s^{-2}.

It must be noted that, simultaneously with the maximum development of the system in low levels, the deepening of the cyclonic perturbation in upper levels ceases (Fig. 9e) and it corresponds, as expected, to an increase of the anticyclonic vorticity as it is observed in Figure 10. This change in the tendency of the vorticity is then associated to the divergence effect (Fig. 12c).

Coming back to Figure 9, the largest deepening occurs at 850 hPa reaching values of relative vorticity lower than -24×10^{-5} s^{-1}. But the first notable cyclonic intensification that initiate this extraordinary deepening begins with a center located at 68°W at 00 UTC of the 11 November. It continues with a more intense center at 06 UTC located at 62.5°W. For the generation of the centers 11 November as well for the one of November, 12 (located in 55°W at 00 UTC and in 50°W at 06 UTC) the divergence term is determinant. As an example, in Figure 13 shows this term at 06 UTC 11 and 12 November, with values of -15×10^{-9} s^{-2} and -21×10^{-9} s^{-2} respectively, clearly dominating the development. At the same time (06 UTC 12 November) and although it decreases to -7×10^{-9} s^{-2}, the convergence effect remains important at 700 hPa.

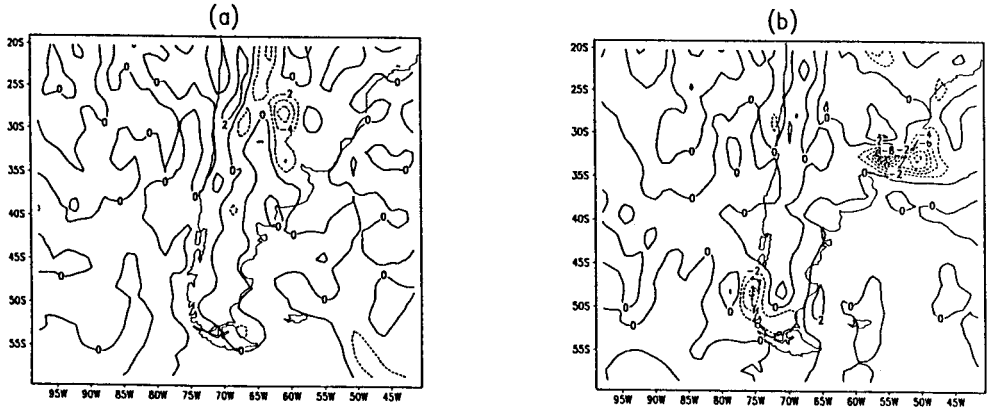

Fig. 13. Divergence term at 850 hPa at: a) 06 UTC 11 November and b) 06 UTC 12 November. Contours are labelled in 2×10^{-9} s^{-2}.

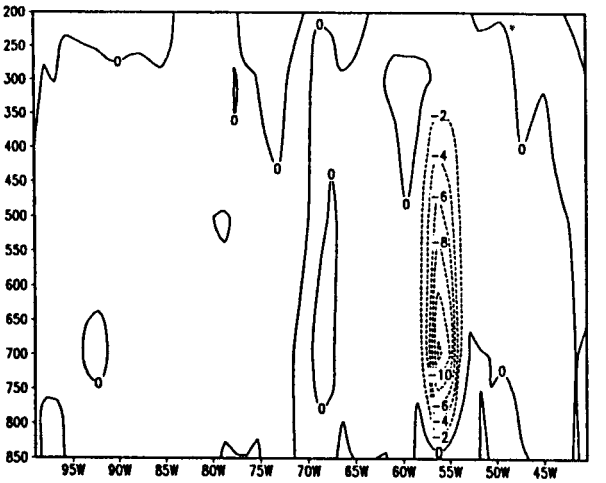

Fig. 14. Zonal vertical cross section at 32.5°S of vertical advection of relative vorticity, at 06 UTC 12 November. Contours are labelled in 2×10^{-9} s^{-2}.

The large vertical velocities observed in Figure 6 are related to the pronounced convergence in this system. On the other hand, as these strong vertical velocities are associated to the large deepening of the system at 850hPa, vertical advection of vorticity at 700 hPa that reached -14×10^{-9} s^{-2} are found at 06 UTC

12 November (Fig. 14). This contribution represents 78% of the system deepening at that level. During the subsequent hours (12 and 18 UTC), the contribution of this term is approximately 50% of the vorticity decrease. That maximum value of the vertical advection of vorticity exceeds in one order of magnitude those given by Grotjahn (1996) in its composition of 15 extratropical cyclones.

This system begins, as already mentioned, at 300 hPa on November 10, but the important intensification occurs in upper as well as lower levels almost simultaneously. At 300 hPa, the horizontal advection of cyclonic vorticity is the most important term followed by the divergence, meanwhile at 850 hPa the convergence results fundamental. At 700 hPa, the vertical advection of vorticity plays a notorious role.

3.2 Thermodynamic factors

3.2.1 The diabatic heat

The effects of the diabatic heating are evaluated from the thermodynamic equation expressed as a function of the potential temperature:

$$\frac{d\theta}{dt} = \frac{\partial\theta}{\partial t} + \mathbf{V}_H \cdot \nabla\theta + \omega\frac{\partial\theta}{\partial p} = \frac{\theta}{C_p T}\frac{\delta Q}{dt} \tag{2}$$

where:

C_p is the specific heat at constant pressure and

δQ non-exact differential of heat

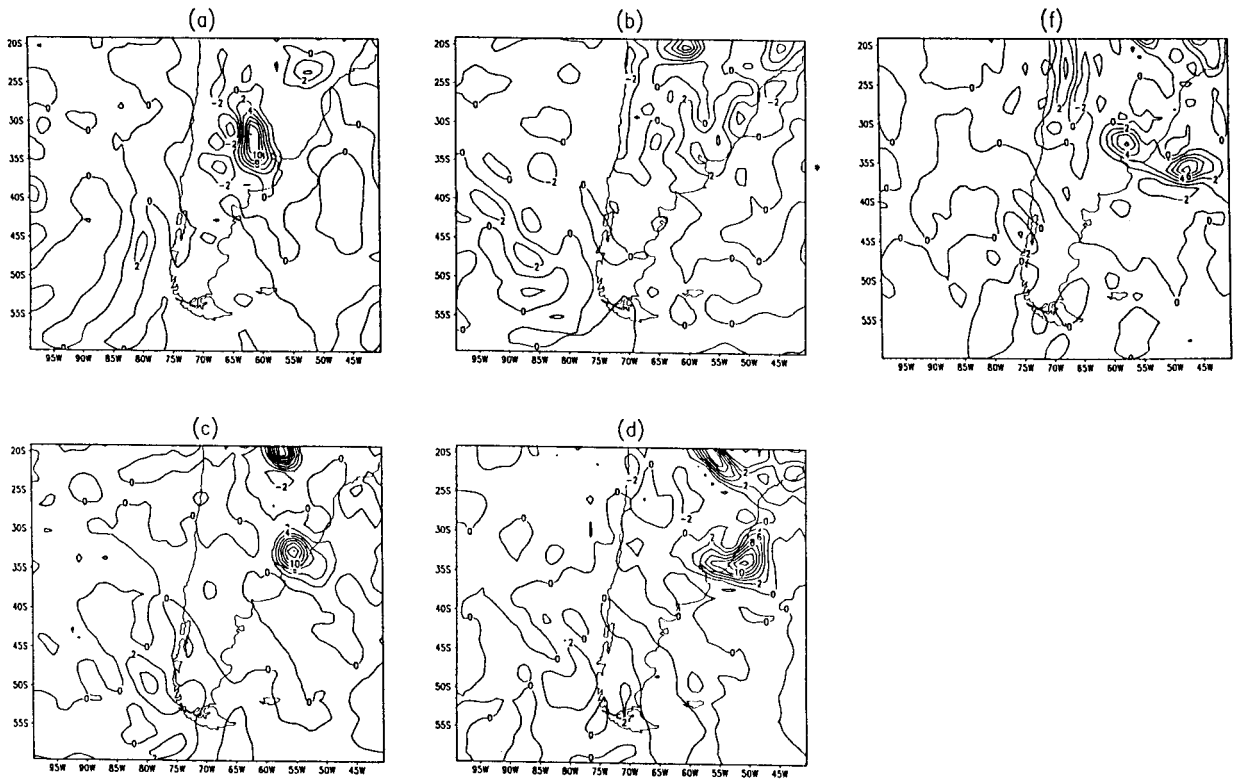

Fig. 15. Individual derivative of θ at 500 hPa at: a) 06 UTC 11 November, b) 00 UTC 12 November, c) 06 UTC 12 Novenber, d) 12 UTC 12 November and e) 18 UTC 12 November. Contours are labelled in 2×10^{-4}K s^{-1}.

The evolution of the individual derivative of θ at 500 hPa is shown in Figure 15 a-f; this level is the one where it reaches the maximum values. In this sequence, very important centers of diabatic heating, 10×10^{-4} K s^{-1}, are visible at 06 UTC 11 November (Fig. 15a), although the maximum value of 16×10^{-4} K s^{-1} is attained at 06 UTC 12 November (Fig. 15c). These magnitudes (Bluestein, 1992) must be related to motions at temporal and spatial scales smaller than the synoptic one. The diabatic heat fields exhibit characteristics that resemble the ones of other variables, at 06 UTC 12 November, they reach maximum values and after 12 UTC elongate to finally form two centers. In the vertical, the diabatic heat covers the whole tropospheric depth with maximum values between 10 and 16×10^{-4} K s^{-4} (Fig. 16). It can be noted that at 06 UTC 11 and 12 November the largest intensifications of the cyclonic system occur.

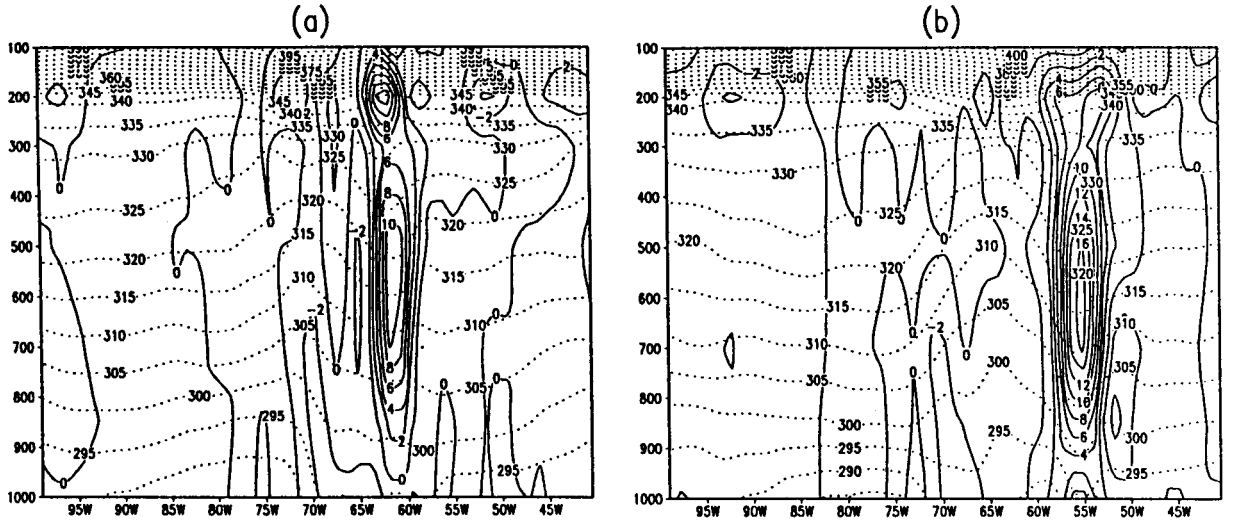

Fig. 16. Zonal vertical cross section at 32.5 °S of individual derivative of θ at a) 06 UTC 11 November and b) 06 UTC 12 November. Contours are labelled in 2×10^{-4} K s^{-1}. Superposed the field of θ (. . . .).

When analyzing the diabatic heat, one more question arises: is only an intensity difference between the maximum diabatic heat, that trigger on November 12 an explosive deepening of the system?

3.2.2 The latent heat

In order to evaluate the latent heat release, the following approximation is used:

$$\frac{1}{C_p}\frac{dQ_v}{dt} \approx -\frac{L_v}{C_p}\frac{dq}{dt} = -\frac{L_v}{C_p}\left(\frac{\partial q}{\partial t} - \nabla \cdot (\mathbf{V}q) + q\nabla \cdot \mathbf{V}\right) \tag{3}$$

where:

Q_v is the latent heat release,

q is the specific humidity and

L_v latent heat of condensation.

It is found that latent heat plays a dominant role in the total diabatic heat. For the humidity convergence at 850 hPa values of -12×10^{-9} s^{-1} and 18×10^{-9} s^{-1} are present at 06 UTC 11 and 12 November, respectively (Fig. 17). Besides, for 06 UTC of the day 11 as well as for 06 and 12 UTC of the day 12 the latent heat release is greater that the total diabatic heat. Figure 18 shows, for one point at 32.5°S and 56°W, the vertical distribution of these variables at 06 UTC 12 November. The absorbed heat by fusion may explain the difference between these two heat values at the 500/700 hPa layer. This result is in agreement

with the formulation of Lau and Lau (1992) who show that the latent heat perturbations largely exceed those of the diabatic heat.

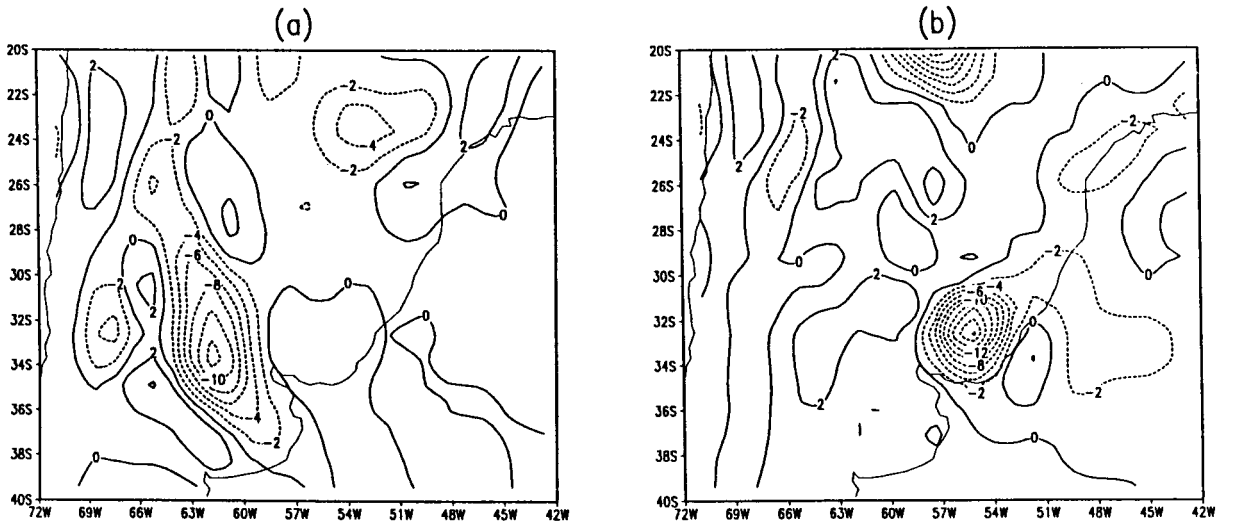

Fig. 17. Water-vapor flux convergence at 850 hPa, at: 06 UTC 11 November and b) 06 UTC 12 November. Contours are labelled in 2×10^{-9} s^{-1}.

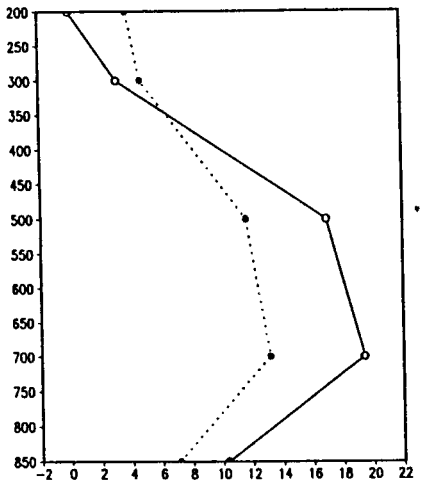

Fig. 18. Vertical distribution of the diabatic heat (—) and latent heat (. . . .) at 32.5°S and 56°W, at 06 UTC November. Units are labelled in 10^{-4}K s^{-1}.

In Figure 9, the increase of the cyclonic vorticity at 850 hPa is clearly visible and, as already mentioned, its weakening towards upper and lower levels of the atmosphere. This results in an increase in the 850/700 hPa thickness values. The vorticity difference between these two levels of the cyclonic system for 12 November doubles the corresponding to 11 November. In order to investigate the causes of the remarkable increase in the thickness value that occurs in the system center at 06 UTC, the different terms of the thermodynamic equation are compared:

$$\frac{\partial T}{\partial t} = -\mathbf{V}_H \cdot \nabla T + \omega \left(\frac{1}{C_p} \frac{RT}{p} - \frac{\partial T}{\partial p} \right) + \frac{1}{C_p} \frac{\delta Q}{dt} \tag{4}$$

where R is the constant of dry air.

Results show that the changes in temperature due to horizontal advection represent a contribution lower than 1×10^{-4} K s^{-1} at 850 hPa and 700 hPa (Fig. 19). The effects due to the difference between adiabatic work and vertical advection of temperature, can be see in Figure 20. This term produces a local temperature decrease at the same levels and its intensity increases with increasing height (from -8×10^{-4} K s^{-1} to -14×10^{-4} K s^{-1}). Finally, in order to complement the comparison between the terms of the equation, the diabatic heat in the 850 y 700 hPa levels is shown in Figure 21; the maximum values at these two levels increase from 6×10^{-4} K s^{-1} to 14×10^{-4} K s^{-1}.

At 850 hPa the net effect of the three terms in the center of the system at 06 UTC imply a local temperature change of -1×10^{-4} K s^{-1}, meanwhile at 700 hPa, the local temperature change is 1×10^{-4} K s^{-1} due to a larger increase of the diabatic heat with height.

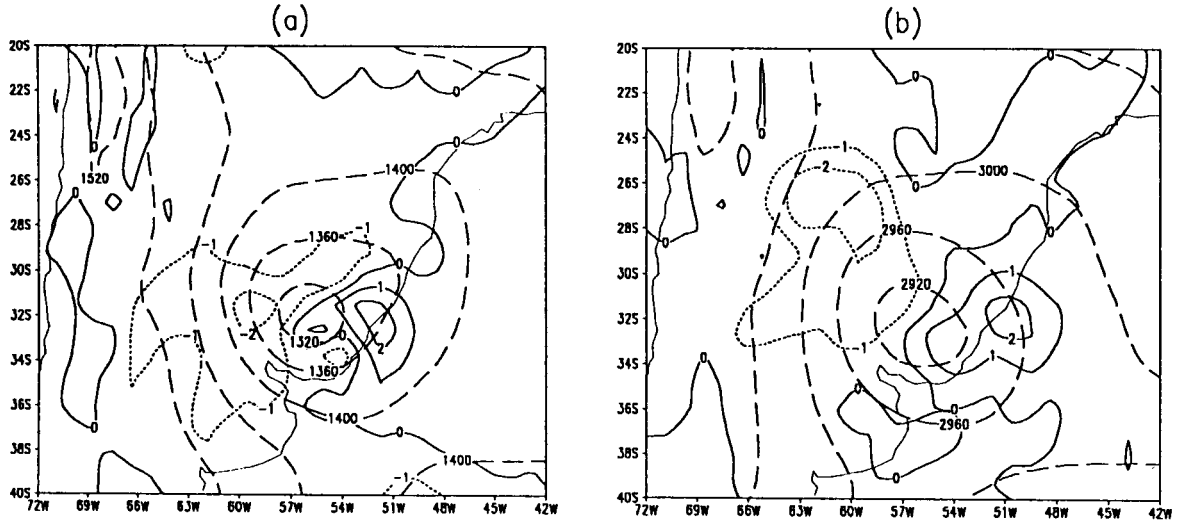

Fig. 19. Horizontal advection of T at 06 UTC 12 November: a) at 850 hPa and b) at 700 hPa. Contours are labelled in 1×10^{-4}K s^{-1}. Superposed geopotential height (- - -) for indicating the position of the system.

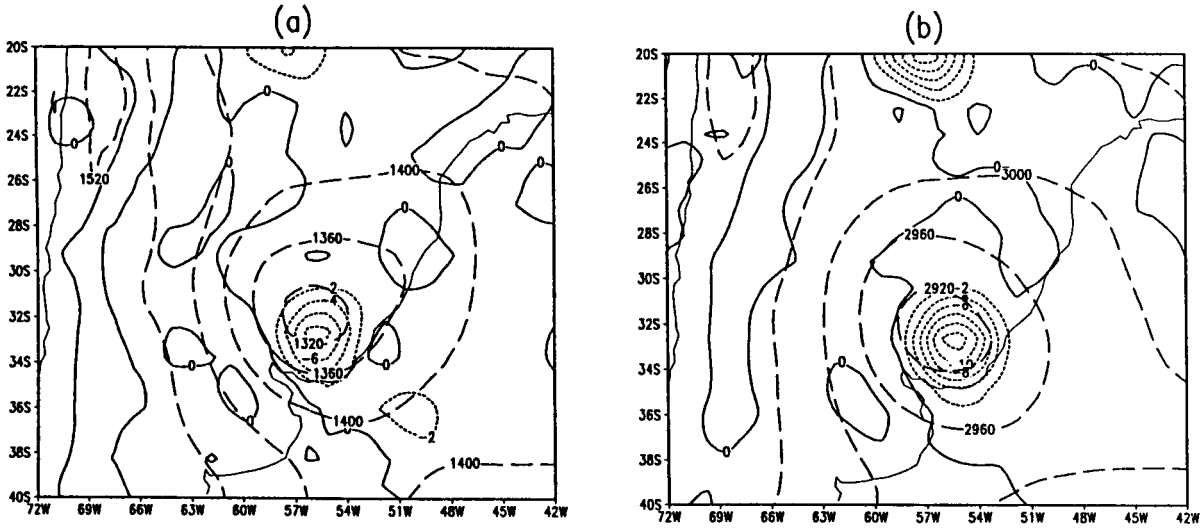

Fig. 20. Static stability effect at 06 UTC 12 November: a) at 850 hPa and b) at 700 hPa. Contours are labelled in 2×10^{-4}K s^{-1}. Superposed geopotential height (- - -) for indicating the position of the system.

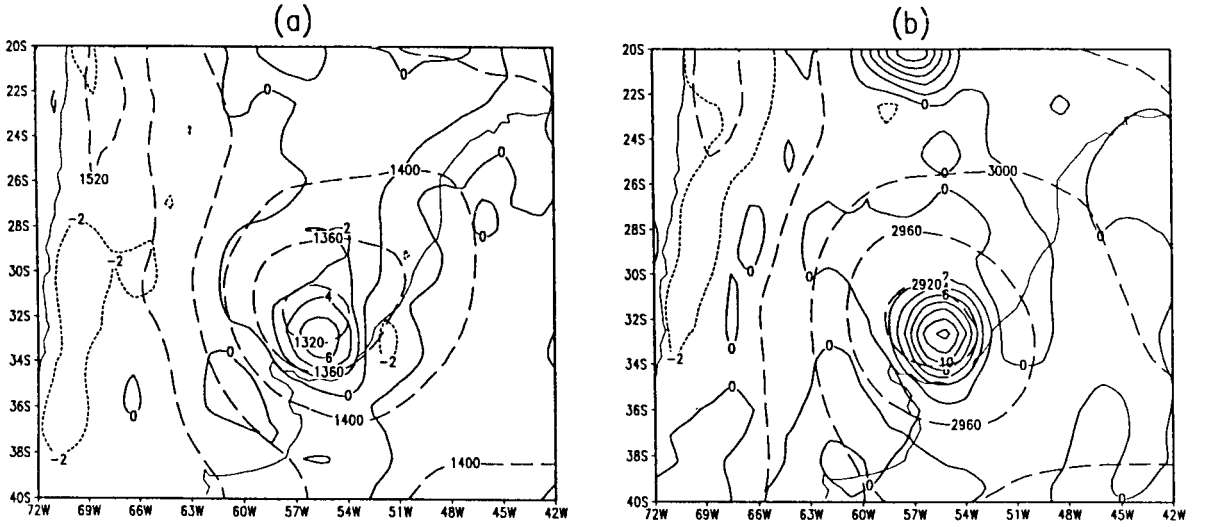

Fig. 21. Diabatic heat effect at 06 UTC 12 November: a) at 850 hPa and b) at 700 hPa. Contours are labelled in 2×10^{-4}K s^{-1}. Superposed geopotential height (- - -) for indicating the position of the system.

4. Behavior of the potential vorticity

It is well known that the potential vorticity can be considered a powerful variable for analysis, as it combines the thermodynamic and dynamic elements of a system. Therefore, in order to evaluate the influence of the heat release in this case study, the terms involving the individual derivative of θ are compared to the horizontal advection of potential vorticity, associated with the conservation of P in a dry adiabatic process. The equation is written as a function of the local changes, neglecting friction effects (Bluestein, 1992):

$$\frac{\partial P}{\partial t} = -\mathbf{V} \cdot \nabla_\theta P - \left(\frac{d\theta}{dt}\right) \frac{\partial P}{\partial \theta} + P \frac{\partial}{\partial \theta}\left(\frac{d\theta}{dt}\right) + \frac{1}{\sigma} \mathbf{k} \cdot \frac{\partial \mathbf{V}}{\partial \theta} \times \nabla \left(\frac{d\theta}{dt}\right) \tag{5}$$

with:

$$P = -g(\zeta_\theta + f)\partial\theta/\partial p \tag{6}$$

where:

P is the potential vorticity,

g the gravitational acceleration,

ζ_θ the vertical component of the relative vorticity in isoentropic coordinates,

$\sigma = -1/g(\partial p/\partial\theta)$ and

$\mathbf{k}$ the vertical versor.

At low levels (305 K), the diabatic term prevails at 06 UTC, 11 November as well as at 12 November. According to the theoretical model of the diabatic term effect, in Figure 18, it is strongly contributing below the 700 hPa level with cyclonic vorticity, while in upper levels, its effect is inverse. Thus, on November 12, the diabatic term produces a decrease of P of -11×10^{-5} UPV s^{-1} at 305 K (Fig. 22), meanwhile the other terms are at least four times smaller. The diabatic term at 11 November reaches a value of -5×10^{-5} UPV s^{-1}, although the ratio with the other terms is similar to the one of November, 12.

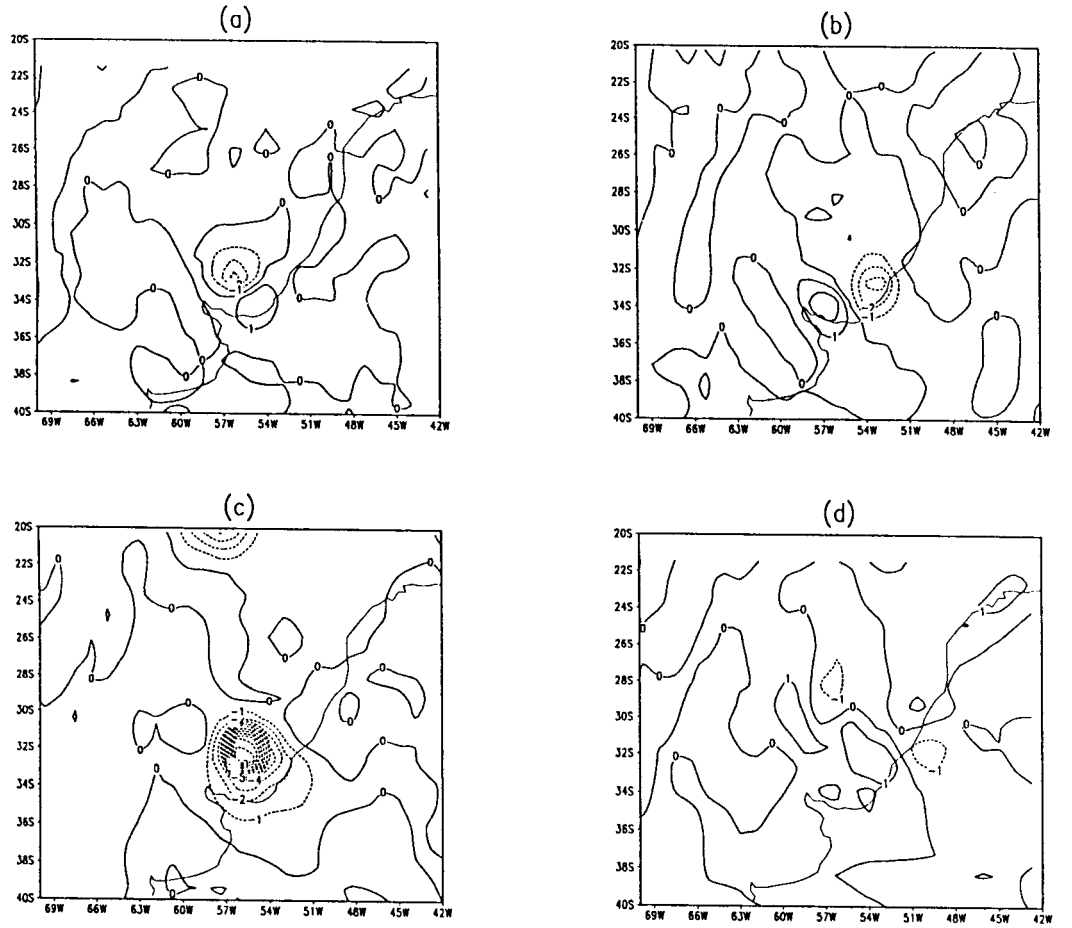

Fig. 22. At 350 K, at 06 UTC 12 November: a) vertical advection of potential vorticity (P), b) twisting term, c) diabatic term, and d) horizontal advection of P. Contours are labelled in 2×10^{-5}UPV*s^{-1}.

At upper levels the fields exhibit different characteristics. The diabatic heat is important increasing anticyclonic potential vorticity. The contribution of the other terms is comparable, the vertical advection of potential vorticity terms and twist term acting in the same sense, while the horizontal advection contributes with cyclonic vorticity (Fig. 23). As a net result, the depletion of cyclonic vorticity at upper levels is observed.

During November 11, the diabatic term reaches a maximum at 325 K depleting cyclonic potential vorticity, while the vertical advection contributes to increase the cyclonic potential vorticity with negligible effects of the other terms. At 330 K, the terms related to diabatic heat decreased and the horizontal advection has an anticyclonic contribution eastwards of the system and a cyclonic one westwards.

According to the previous paragraphs, the anticyclonic contribution that occurs at upper levels as a result of the diabatic heat requires a cyclonic vorticity field intense enough to preserve this condition. The potential vorticity fields corresponding to 330 K for 06 UTC 11, and 12 November are shown in Figure 24. It is clear that at 11 November, the potential vorticity within the heat release zone is completely depleted by this mechanism. Even when the diabatic mechanisms are more intense on the 12$^{\text{th}}$, the potential vorticity remains cyclonic. Figure 4 shows the relative vorticity fields at 300 hPa for 06 UTC November 11 and 12.

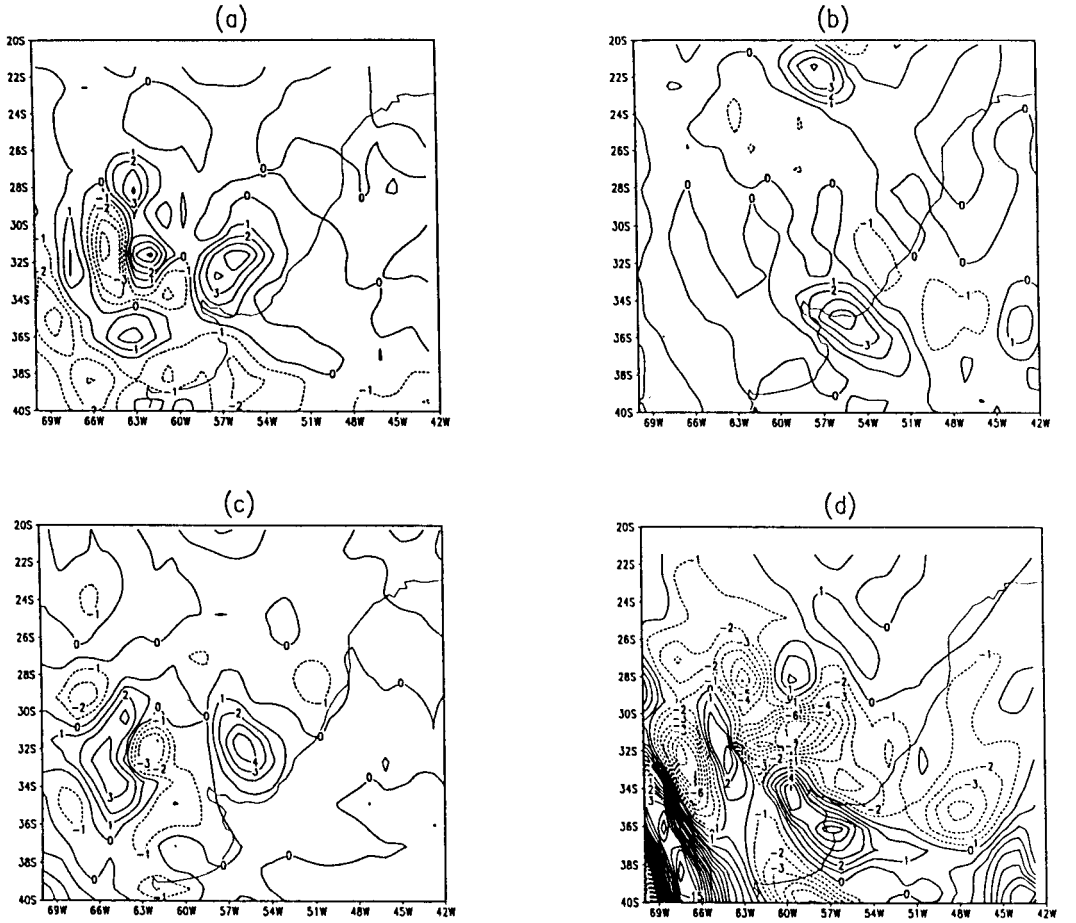

Fig. 23. At 330 K, at 06 UTC 12 November: a) vertical advection of P, b) twisting term, c) diabatic term, and d) horizontal advection of P. Contours are labelled in 2×10^{-5}UPV s^{-1}.

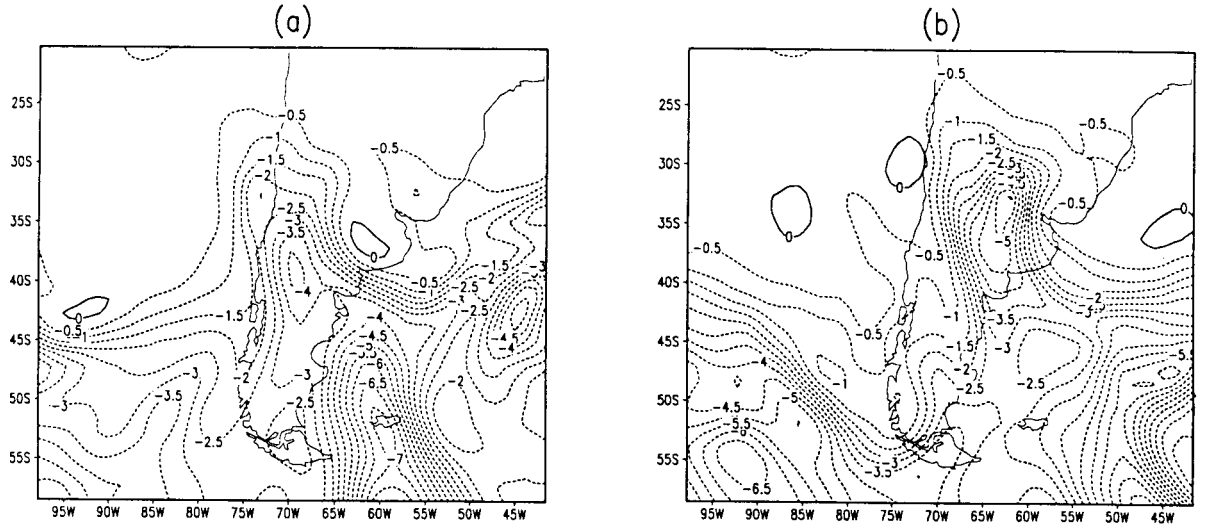

Fig. 24. Potential vorticity at 330 K, at: a) 06 UTC 11 November and b) 06 UTC 12 November. Contours are labelled in 1UPV.

5. Conclusions

The cyclonic perturbation first appears in upper levels at 06 UTC 10 November, and twelve hours later it is visible at all of the 7 levels. At 300 hPa, the process begins with advection of cyclonic vorticity during the 11 November, and afterwards the divergent term associated to the development at the other levels become more important.

The system is full of diabatic processes that start on November 11, with values that correspond to scales smaller than the synoptic one.

The largest deepening occurs at 850 hPa and it is related to an intense convergence field. This fact is closely related to the intense upward motion, that in conjunction with the advection of warm and humid air from the northeast and toward the cyclone center produces condensation and latent heat release, and a 850/700 hPa thickness typical of a warm cyclone. According to Sanders and Gyakum (1980), the energy source of those systems of rapid development is over the sea (Sea Surface Temperature and its strong gradients). In this case as surface temperatures where the cyclogenesis takes place are relatively low, the energy has to be advected from northeast.

At 700 hPa, the most important mechanisms result to be the convergence and the vertical advection of cyclonic vorticity, playing the latter a relevant role when the system attains its maximum development.

Through the analysis of the potential vorticity, it became clear that the diabatic term is responsible for the depth and fast development of this cyclogenesis at low levels. It occurred with a cyclonic system at upper levels, strong enough to compensate the anticyclonic effects of the diabatic heat in these levels.

Acknowledgements

The author wants to thank Dr. Erich Lichtenstein for his good disposition, useful discussions and comments, and his constant encouragement and to Lic. Claudia Simionato for her comments about the English version of this paper. This study has been supported by the project UBA TW22.

REFERENCES

Bluestein, H. B., 1992. Synoptic-Dynamic Meteorology in Midlatitudes. Vol. II, Oxford University Press.

Bolton, D., 1980. The computation of Equivalent Potential Temperature, *Mon. Wea. Rev.,* **108,** 1046-1953.

Gerald, C. F., 1978. Applied Numerical Analysis. Addison-Wesley Publishing Company

Grotjahn, R., 1996. Vorticity Equation Terms for Extratropical Cyclones. *Mon. Wea. Rev.,* **124**, 2843-2858.

Gordillo, S. B., A. F. Belohlawek, M. J. García y M. E. Saluzzi, 1991. Estudio retrospectivo de una rápida y severa ciclogénesis que produjo cuantiosos daños socioeconómicos en la zona ribereña del Río de la Plata. Anales del CONGREMET VI, págs. 121-122.

Lau, K. H. and N. C. Lau, 1992. The Energetics and Propagation Dynamics of Tropical Summertime Synoptic-Scale Disturbances, *Mon. Wea. Rev.*, **120**, 2523-2539.

Ruscher, P. H. and T. P. Condo, 1996. Development of Rapidly Deepening Extratropical Cyclone over Land. Part I: Kinematic Aspects, *Mon. Wea. Rev.*, **124**, 1609-1632

Sanders, F. and J. R. Gyakum, 1980. Synoptic-dynamic climatology of the "bomb, *Mon. Wea. Rev.*, **108**, 1589-1606.

Seluchi, M., 1995. Diagnóstico y pronóstico de situaciones sinópticas conducentes a ciclogénesis sobre el este de Sudamérica. *Geofís. Inter.*, Vol. **34**, pp. 171-186.

Seluchi, M. and A. C. Saulo, 1998. Possible mechanisms yielding an explosive coastal cyclogenesis over South America: experiments using a limited area model. *Australian Magazine,* Vol. **47**, 309-320.